Chapter 3

Imaging

3.1 Observations

All photometric measurement have been derived from I-band CCD images. The adoption of I band for photometry was mainly dictated by the practical notion that the cluster images contain several galaxies per frame, both of early– and late–type, and thus can be useful for TF application, where the I band is favored for compatibility with G97a,b.

Most of the observations were obtained during three runs with the 0.9m telescope of the Kitt Peak National Observatory (KPNO). A small number of observations in the cluster A2634 was obtained during observing runs with the 1.3m telescope of the Michigan-Dartmouth-MIT (MDM) Observatory (runs 1 and 3 in Table 3.1). Other observations in A2634 were obtained by KPNO staff with the 0.9m telescope during a period of service observations (run 2 in Table 3.1). A few images in the Cancer cluster and in the NGC 383 group were obtained by Riccardo Giovanelli during observing runs allocated for a different project at the KPNO 0.9m telescope (runs 7 and 6, respectively, in Table 3.1). Table 3.1 summarizes all observing runs during which data were obtained for this project, and gives some parameters of the relative instrumental set-ups. The only significant difference between the MDM and the KPNO observations is the much smaller field of view of the 1.3m MDM telescope, when compared with the Ritchey-Cretièn 0.9m KPNO telescope.

All CCD frames were obtained with 600 seconds integration time. For the brightest objects a second frame with shorter integration (200–300 seconds) was necessary, to avoid saturation of the image in the nuclear region of the galaxy. The median effective seeing (measured as the FWHM of the stellar light profile) for the entire data set is 1.6 arcsec. Figure 3.1 shows the distribution of this effective seeing for the galaxy observations. The actual atmospheric seeing might have been smaller at times, but the pixel size with which the majority of the observations were obtained limits the effective seeing to $\simeq$1.2 arcseconds. Given the large field of view of the KPNO 0.9m telescope, and the large density of galaxies in the cluster environments studied here, a complete mapping of the clusters' central regions was obtained, with a mosaic of frames on a regularly spaced grid (except in the case of A2634 and Cancer). Only for the galaxies at the periphery of the various clusters were off-grid pointings used. The panels of Figure 3.2 show the distribution on the sky of all the frames that were obtained. The frames obtained in photometric sky conditions are indicated by the solid line contours, while the dashed

Table 3.1 Imaging observing runs

	Run 1	Run 2, 4–8	Run 3
Telescope	MDM 1.3m	KPNO 0.9m	MDM 1.3m
CCD	Loral2048 (Wilbur)	T2KA	Tek1024 (Charlotte)
Pixels	1024 x 1024	2048 x 2048	1024 x 1024
Read-out noise	6 e^-	4 e^-	4.8 e^-
Gain	1.9 e^-/DU	3.2 e^-/DU	3.45 e^-/DU
Pixel scale	0.63 ”/pixel	0.68 ”/pixel	0.51 ”/pixel
Field of view	11 x 11 arcmin	23 x 23 arcmin	9 x 9 arcmin

	Run 1	Run 2	Run 3
Dates	Sep. 23-25 1992[a]	Aug 18-20 1993[b]	Sep. 8-9 1993[a]
Photometric nights	(3)	0	(2)
Marginal nights	0	3	0
Nr. of galaxies	10	81	6

	Run 4	Run 5	Run 6
Dates	Apr. 14-19 1994	Aug. 31 - Sep. 6 1994	Oct. 8 1994[a]
Photometric nights	3	3	(1)
Marginal nights	1	1	0
Nr. of galaxies	331	228	19

	Run 7	run 8
Dates	Mar. 6 1995[a]	Sep. 24 - Oct. 1 1995
Photometric nights	0	2
Marginal nights	(1)	2
Nr. of galaxies	5	47

[a] Observing run mainly dedicated to a different project; only a small portion of telescope time dedicated to this project.
[b] Service observing by KPNO personnel

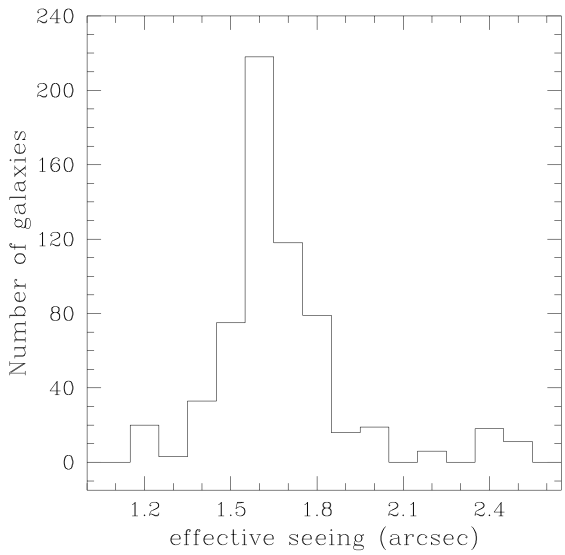

Figure 3.1 The distribution of effective seeing for the galaxy observations. The pixel size of 0.68 arcsec. limits this effective seeing to $\simeq$1.2 arcsec.

line contour identifies those obtained in non-photometric conditions.

Surface photometry has been obtained for all "interesting" objects in all available frames for each cluster, for a total of 631 galaxies. Elliptical, S0 and S0a galaxies have been selected from the images themselves, based on their being potentially good candidates for FP work. Foreground or background objects have been excluded from these samples. A number of galaxies without redshift measurement, but with luminosity and size that make them likely cluster members, have instead been included in the samples. Galaxies in close pairs or multiplets, and galaxies contaminated by bright foreground stars projected over the galaxy or in its immediate vicinity have been rejected, unless a velocity dispersion measurement was already available for the galaxy. Only in these cases has an attempt been made to subtract the contribution of the contaminating object to the observed light distribution (see below). The final samples therefore are not rigorously magnitude (or diameter) limited, but the small amount of incompleteness should not be statistically significant. This is a situation similar to the one encountered when magnitude limited samples are obtained selecting objects on the basis of pre-CCD photometry, which is characterized by relatively large uncertainties.

The panels of Figure 3.3 show the distribution in the sky of all the galaxies for which photometric parameters have been derived. For each cluster the dashed circle has a radius of 1 Abell radius (1 $R_A = 1.5\ h^{-1}$Mpc).

Table A.1 in the appendix lists all the objects for which photometric parameters have been derived. The table is organized as follows:

Col. 1: Galaxy name, using the following galaxy identifiers: if the galaxy is listed in the UGC catalog (Nilson 1973), the UGC number is given; if not, our internal coding number is given.

Cols. 2 and 3: the NGC or IC number, if the galaxy is listed in those catalogs, and the CGCG field and ordinal number within that field, if the galaxy is listed in the CGCG

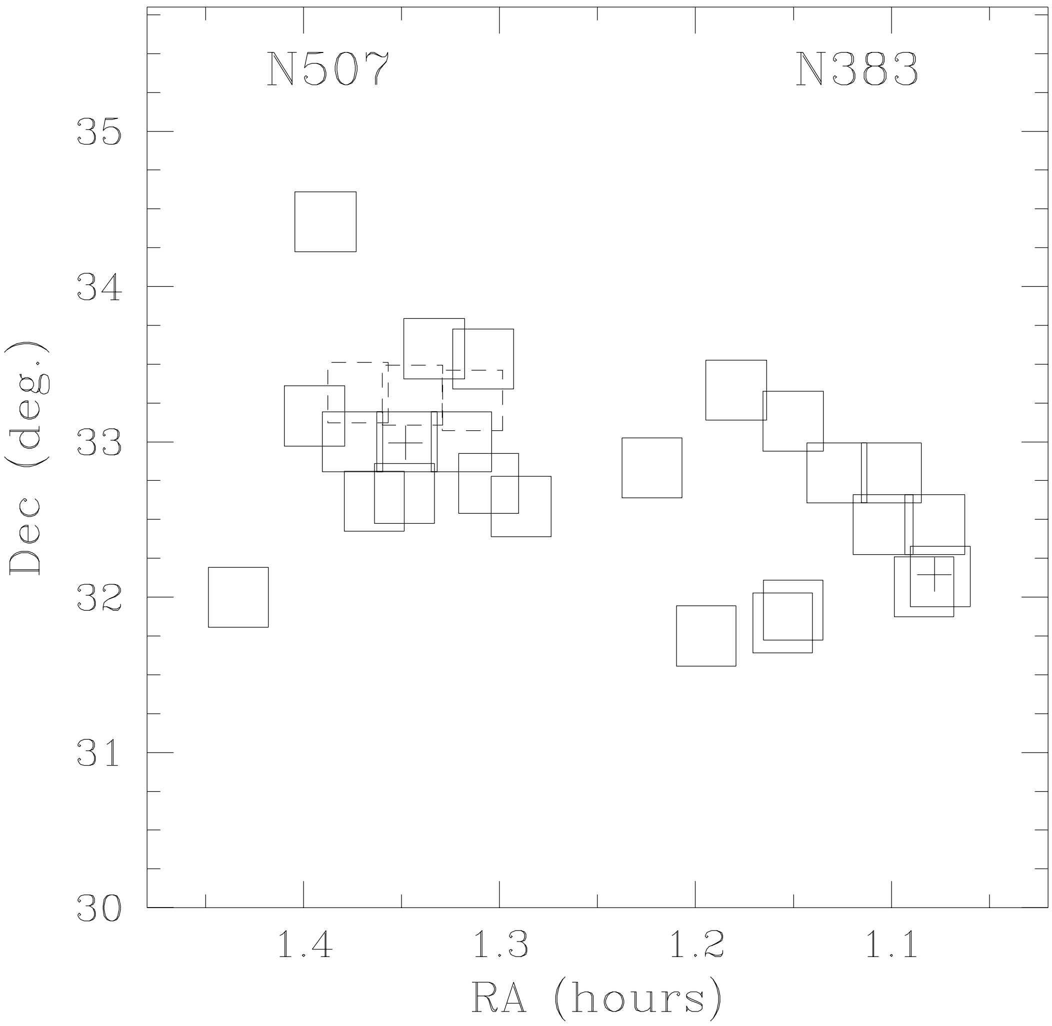

Figure 3.2 The panels in this and the following pages show the distribution on the sky of the CCD frames that were obtained for the photometric observations discussed in this chapter. Frames with a solid line contour were obtained in photometric conditions, while those with a dashed line contour were obtained in non-photometric conditions. In each panel the cross marks the position of the cluster center.

Figure 3.2 (Continued)

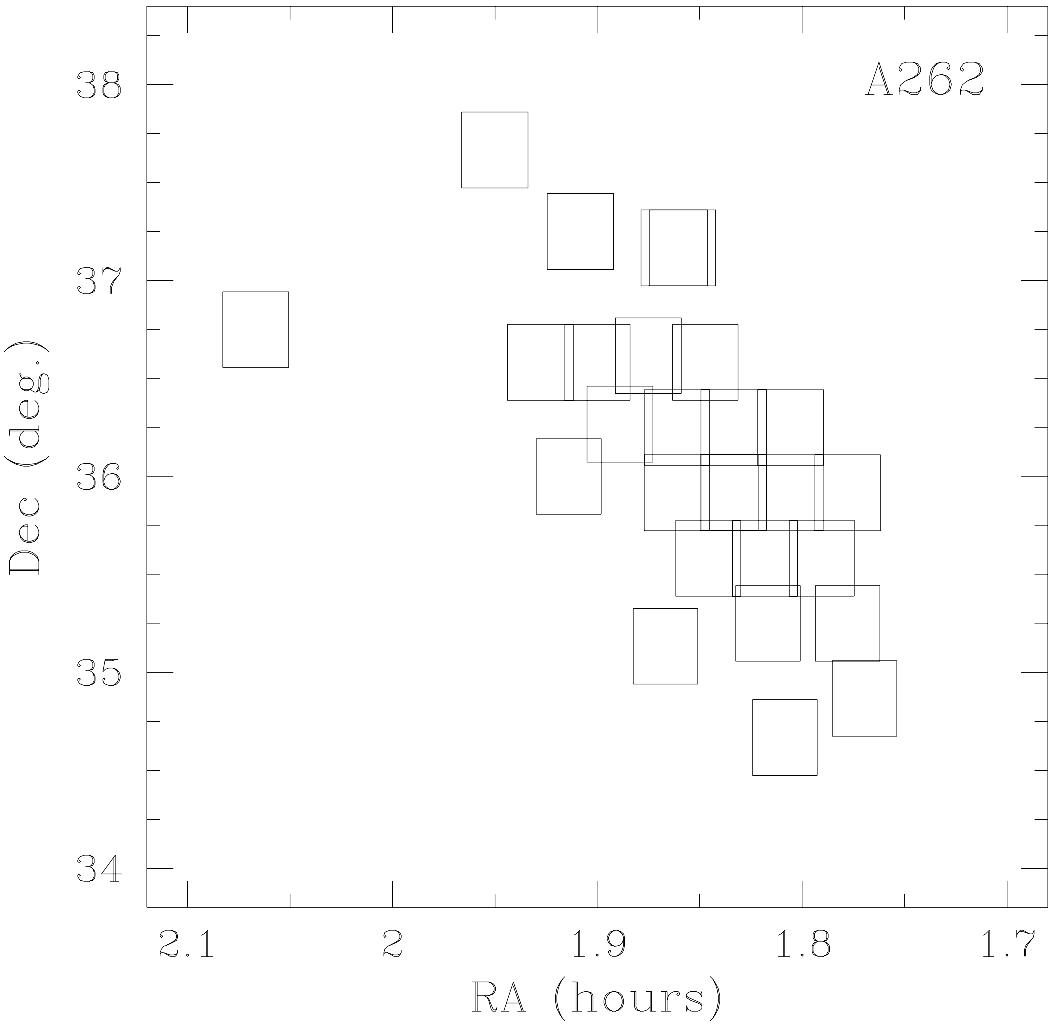

Figure 3.2 (Continued)

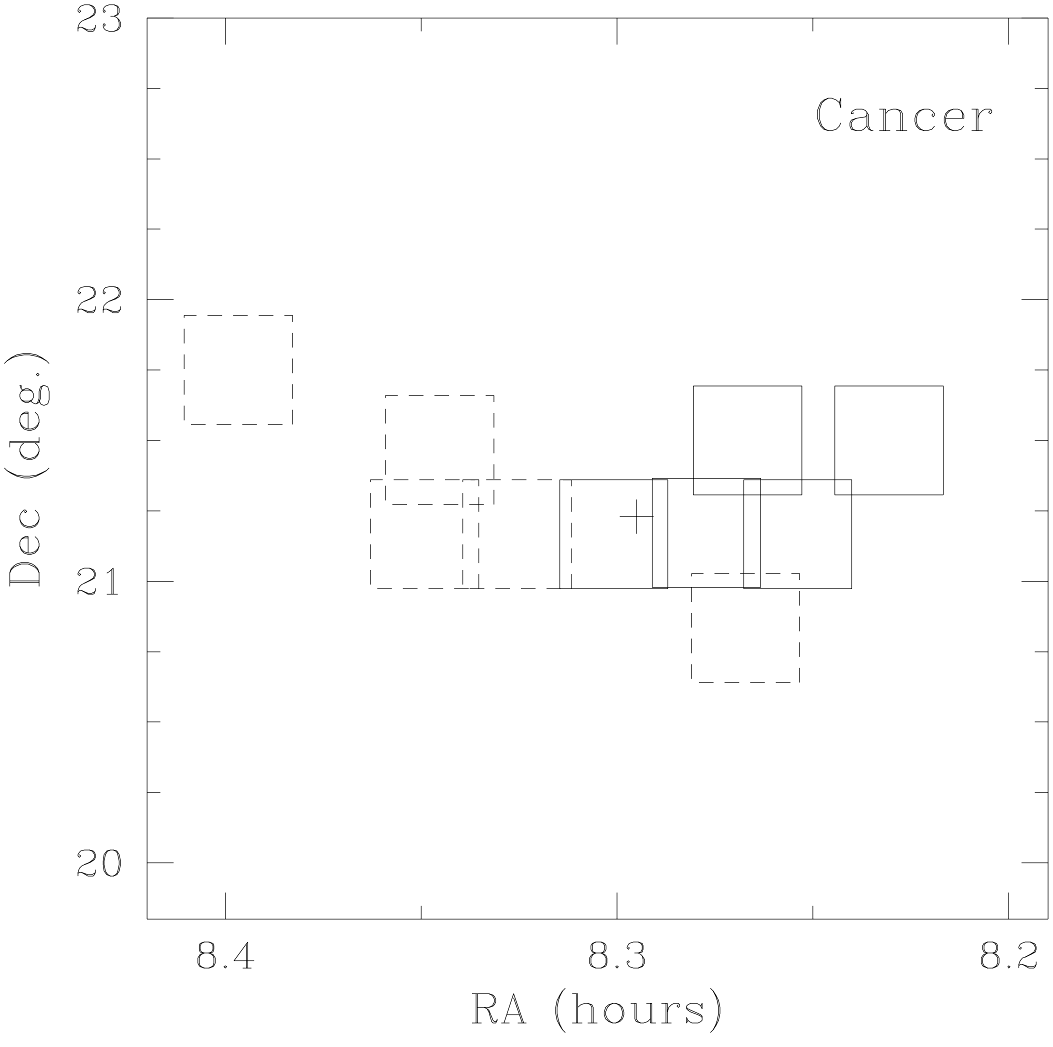

Figure 3.2 (Continued)

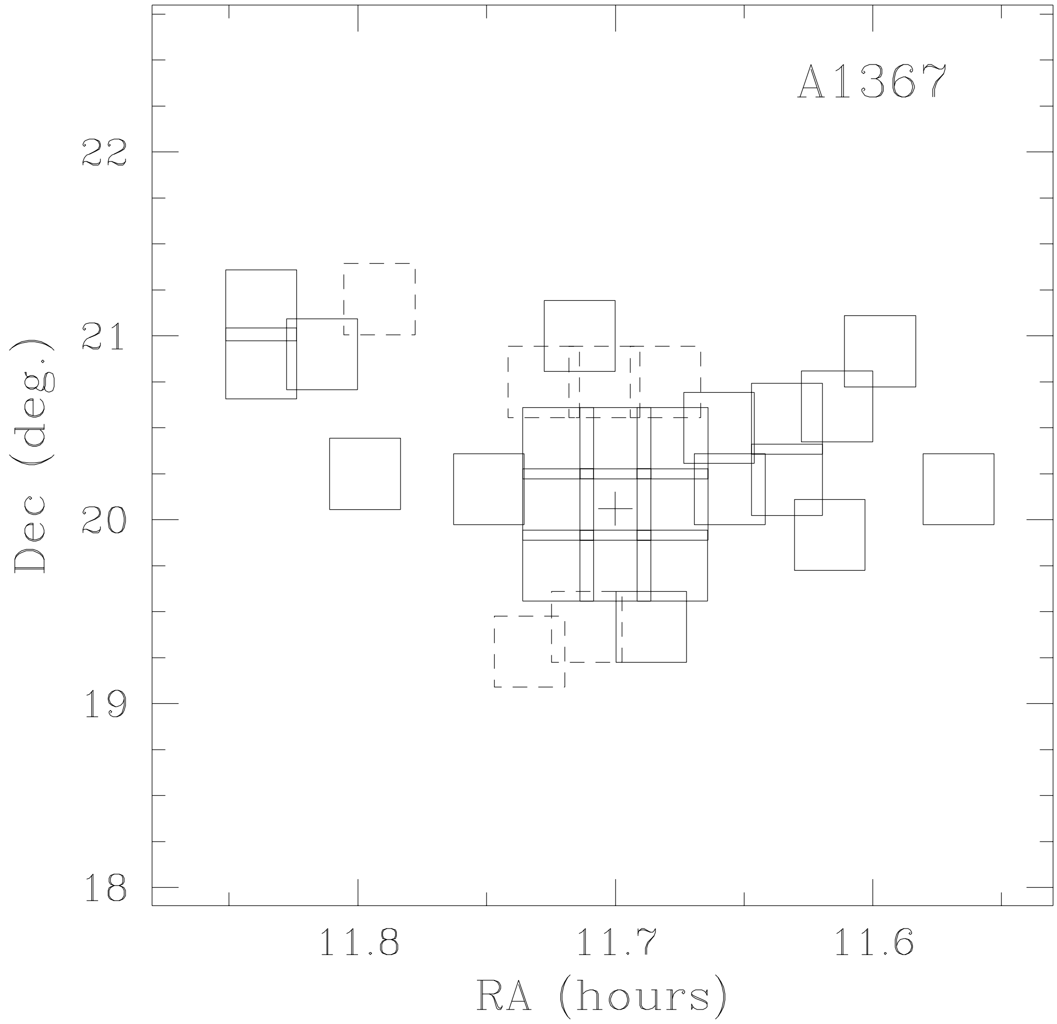

Figure 3.2 (Continued)

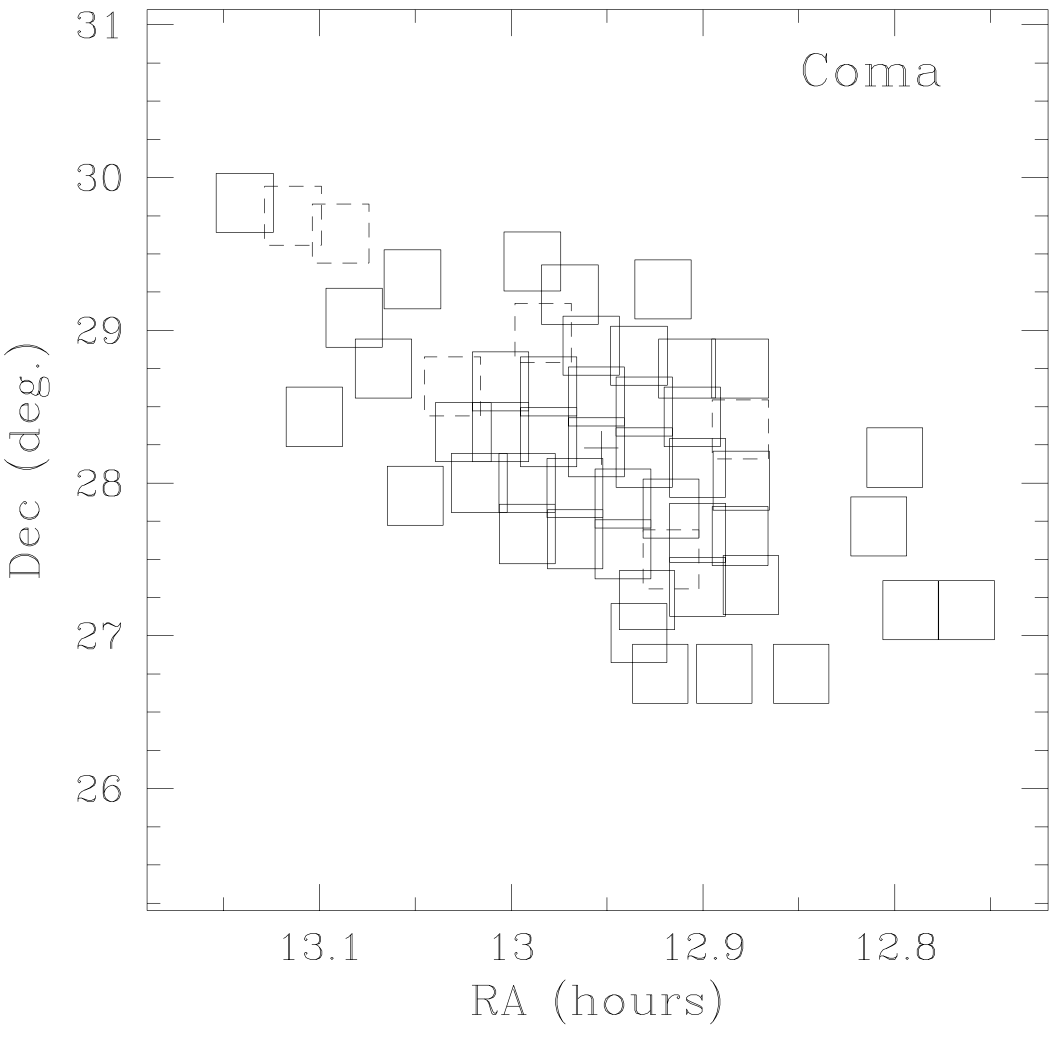

Figure 3.2 (Continued)

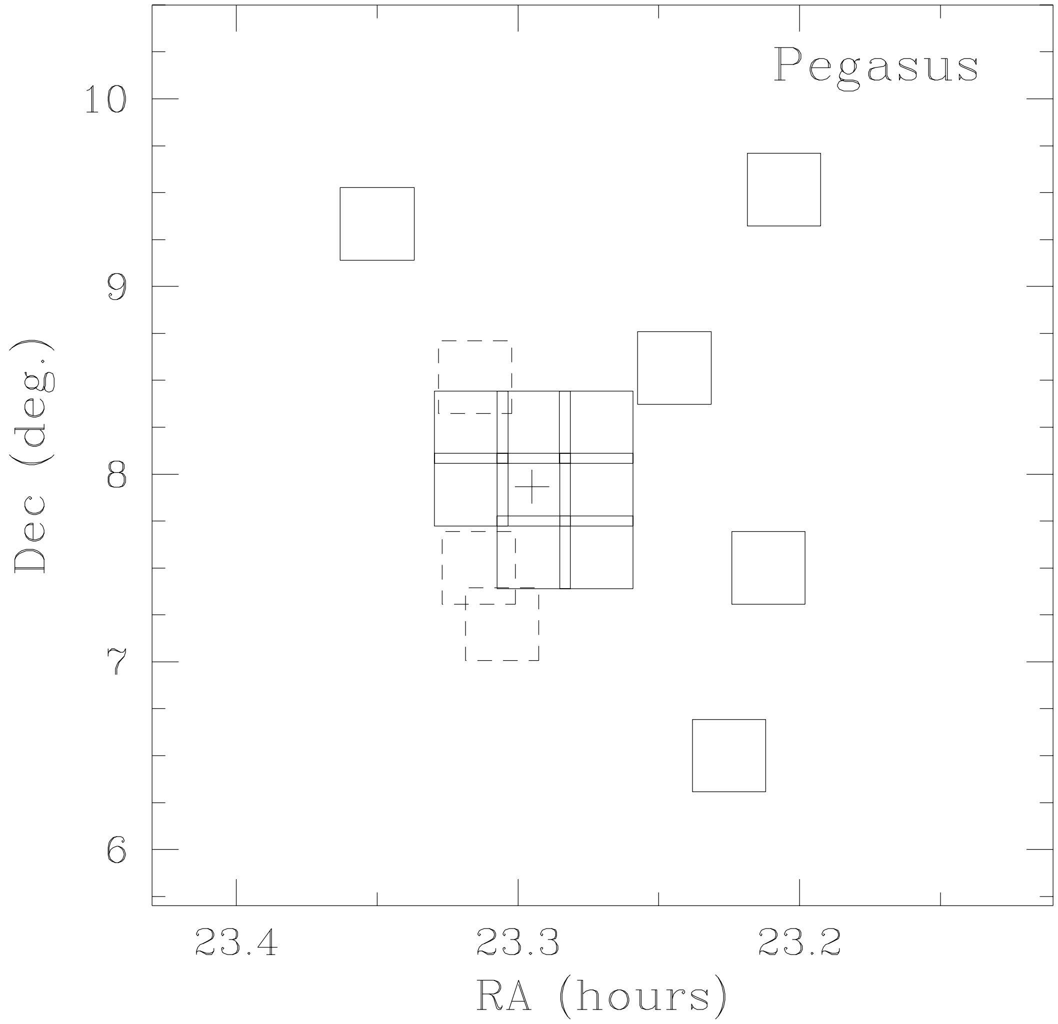

Figure 3.2 (Continued)

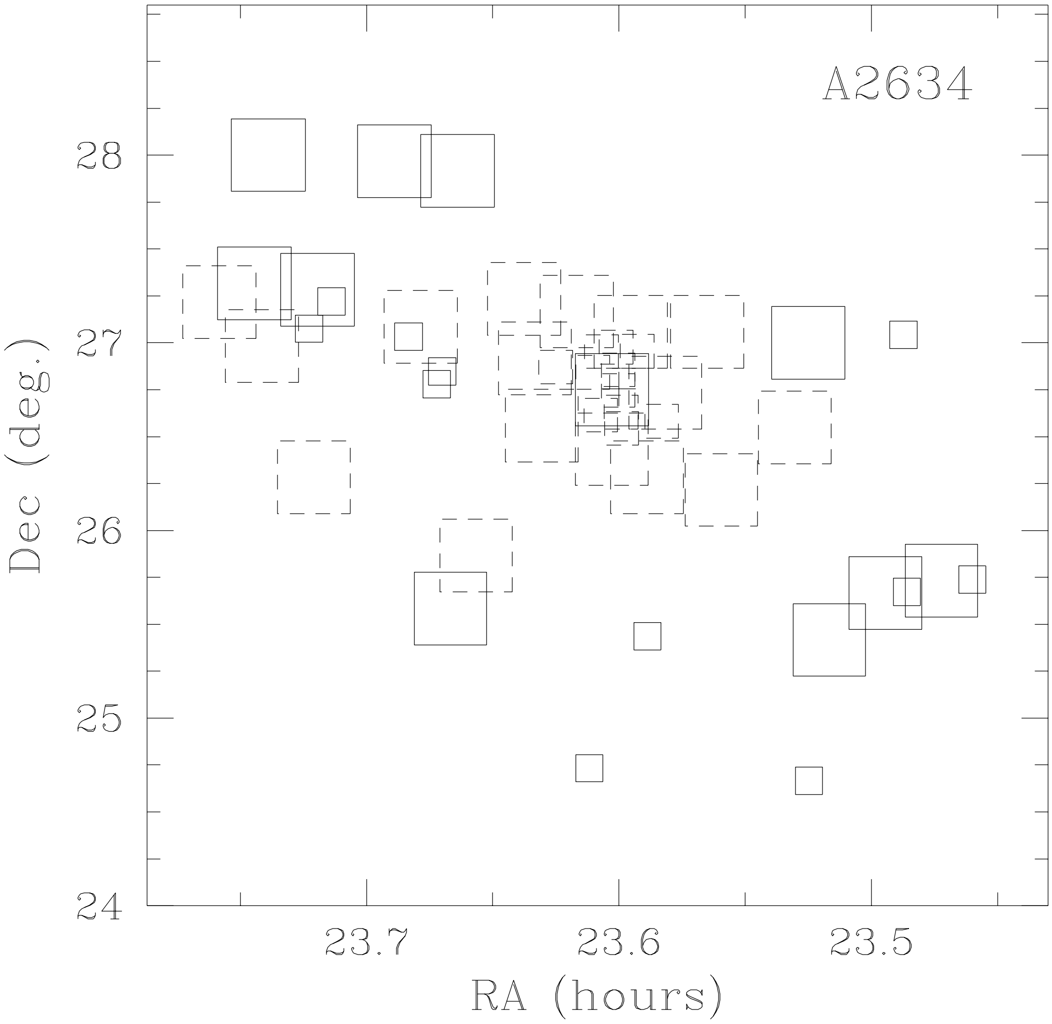

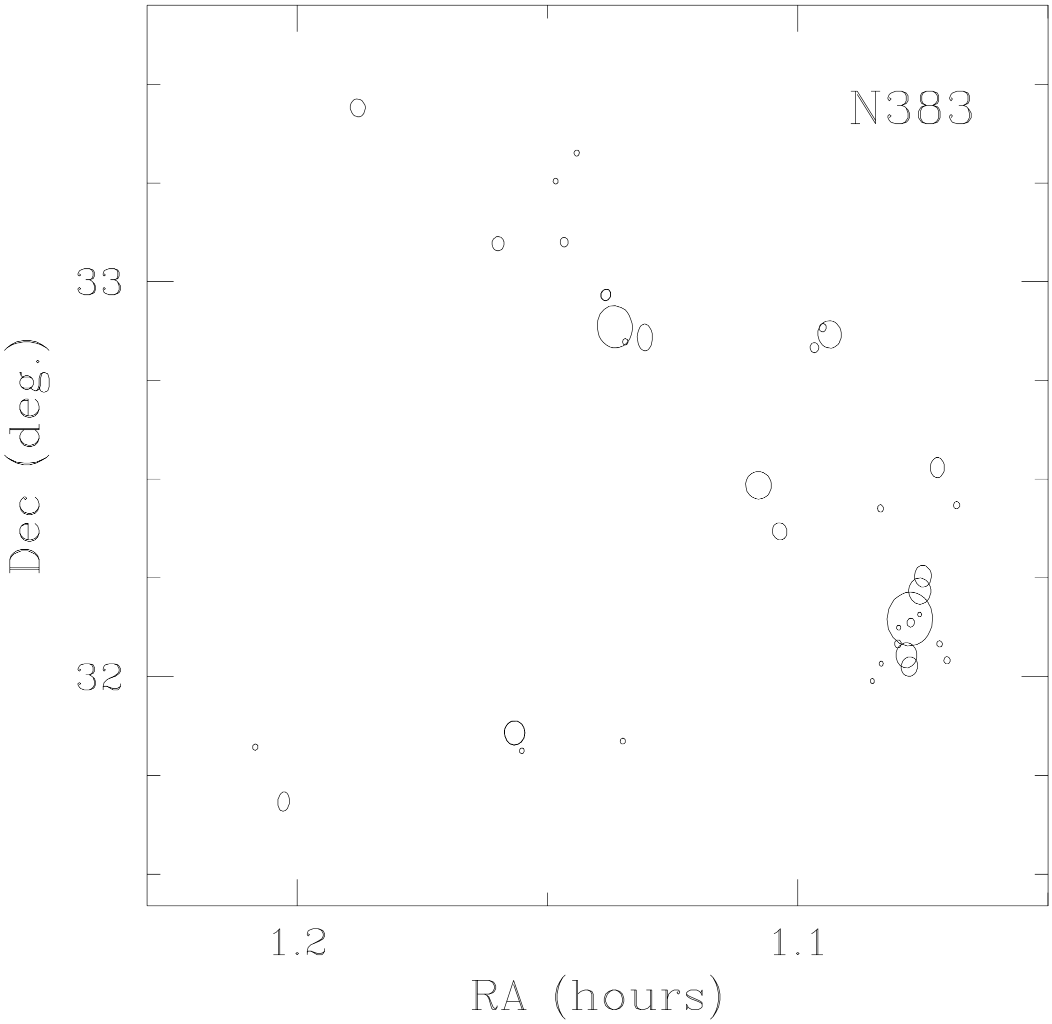

Figure 3.3 The panels in this and the following pages show the distribution on the sky of the galaxies with measured photometric parameters. Each galaxy is marked with an ellipse that corresponds to its isophote measured at 23.5 I band magnitudes per square arcsecond. The ellipses are magnified by a factor $\simeq 1.5$ to increase their visibility. In each panel the dashed concentric circle has a radius of 1 Abell radius (1 $R_A = 1.5\ h^{-1}$Mpc). In the case of NGC383, Cancer and Pegasus, the circle is entirely outside the plotted area.

Figure 3.3 (Continued)

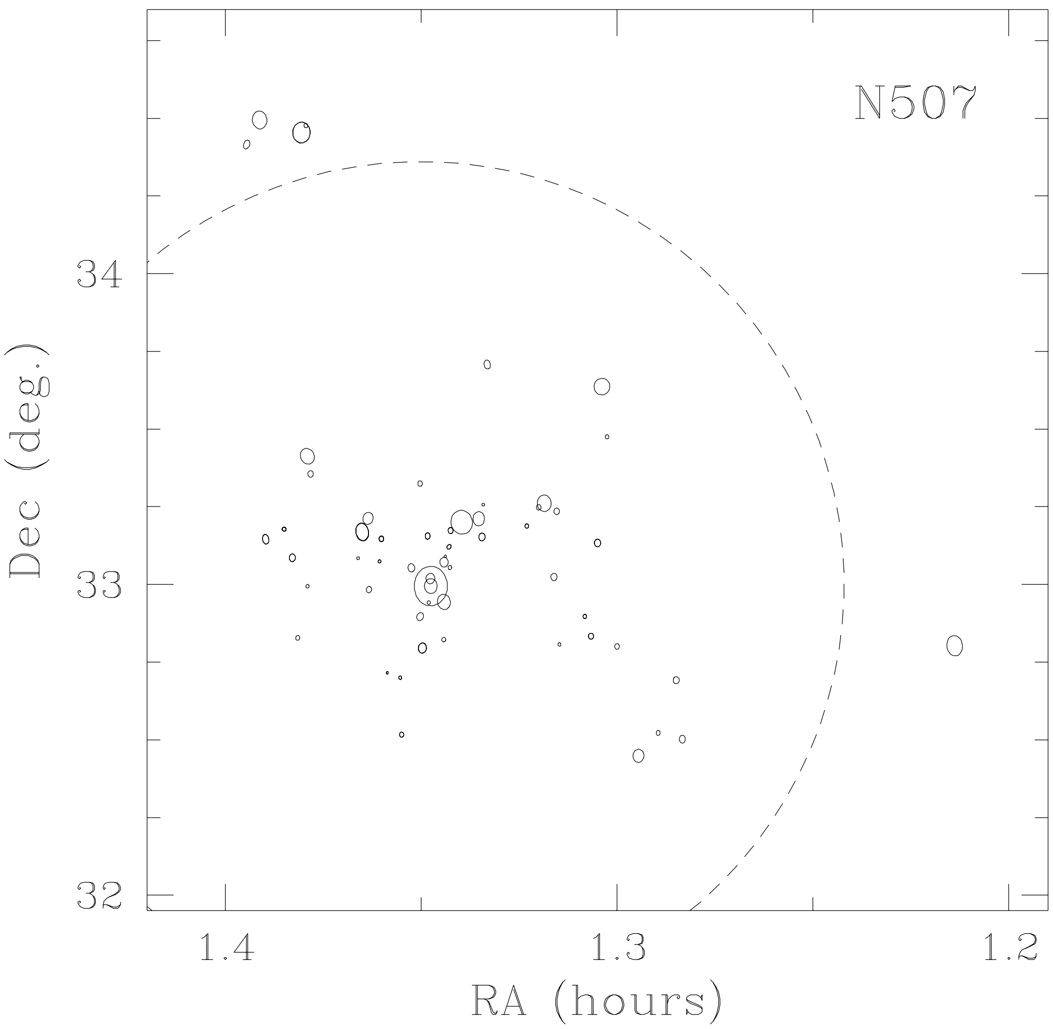

Figure 3.3 (Continued)

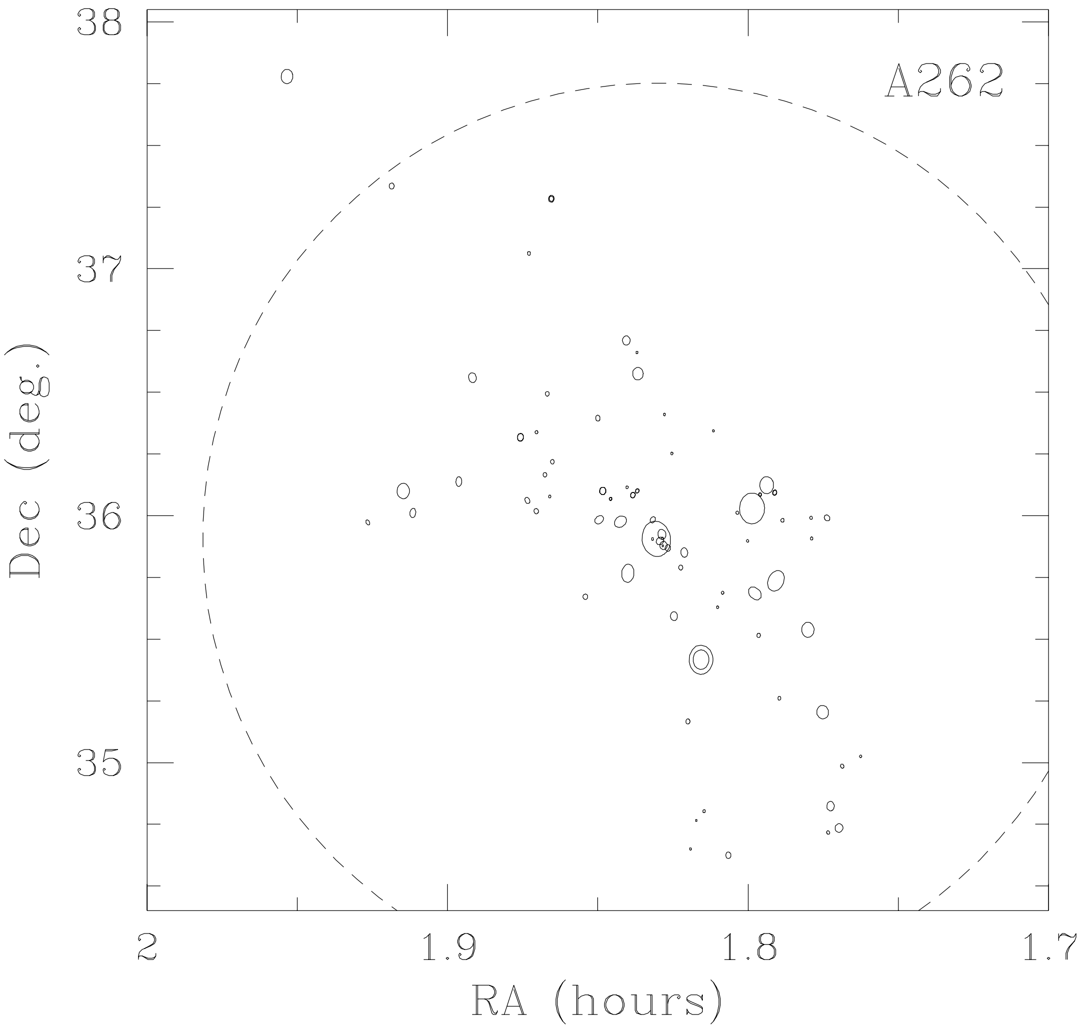

Figure 3.3 (Continued)

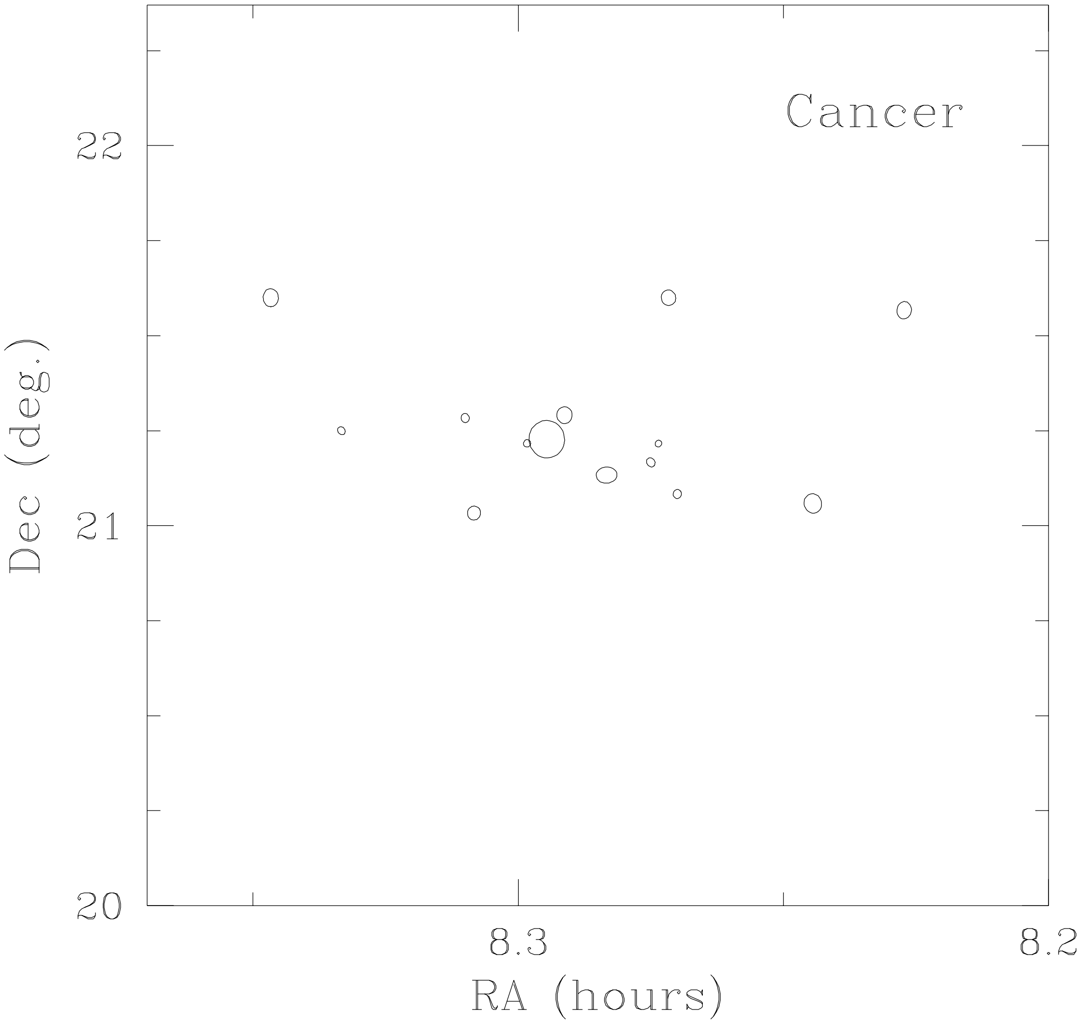

Figure 3.3 (Continued)

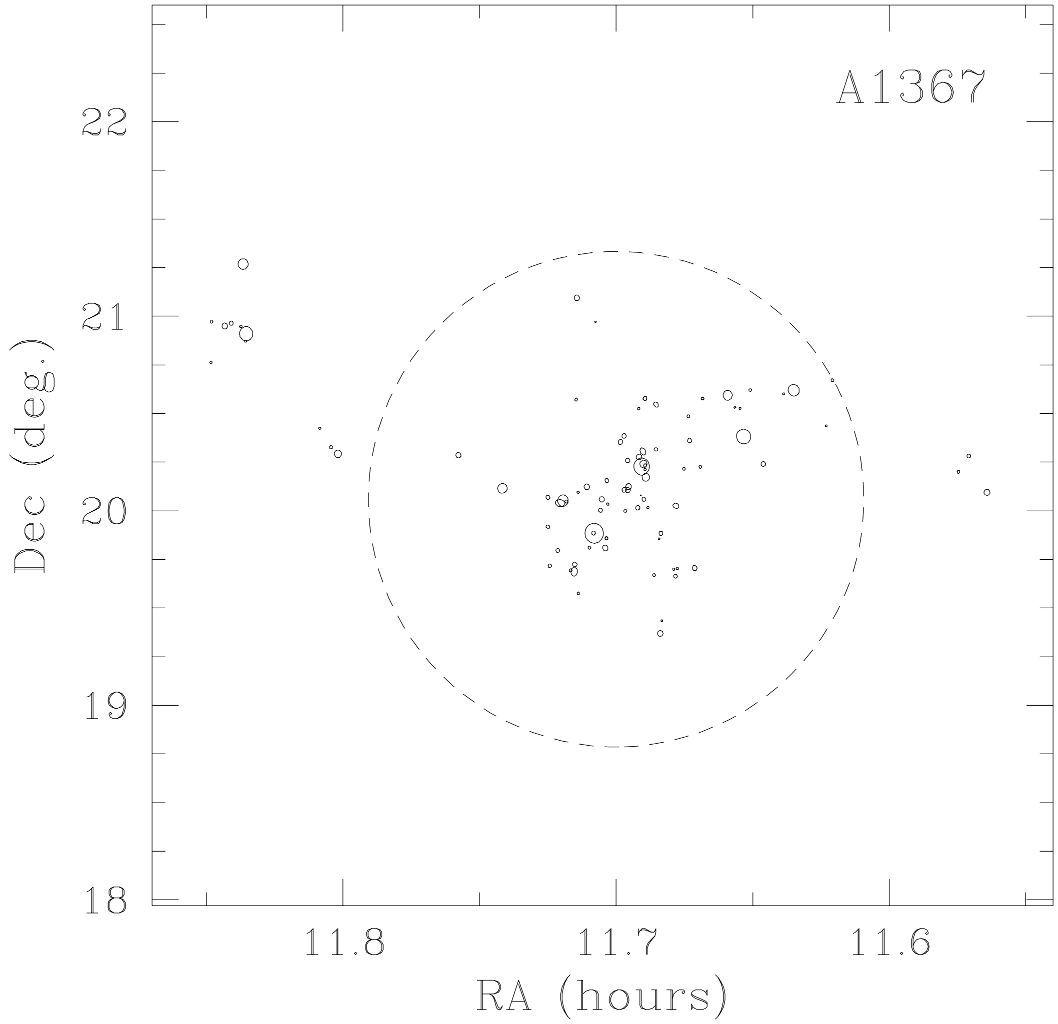

Figure 3.3 (Continued)

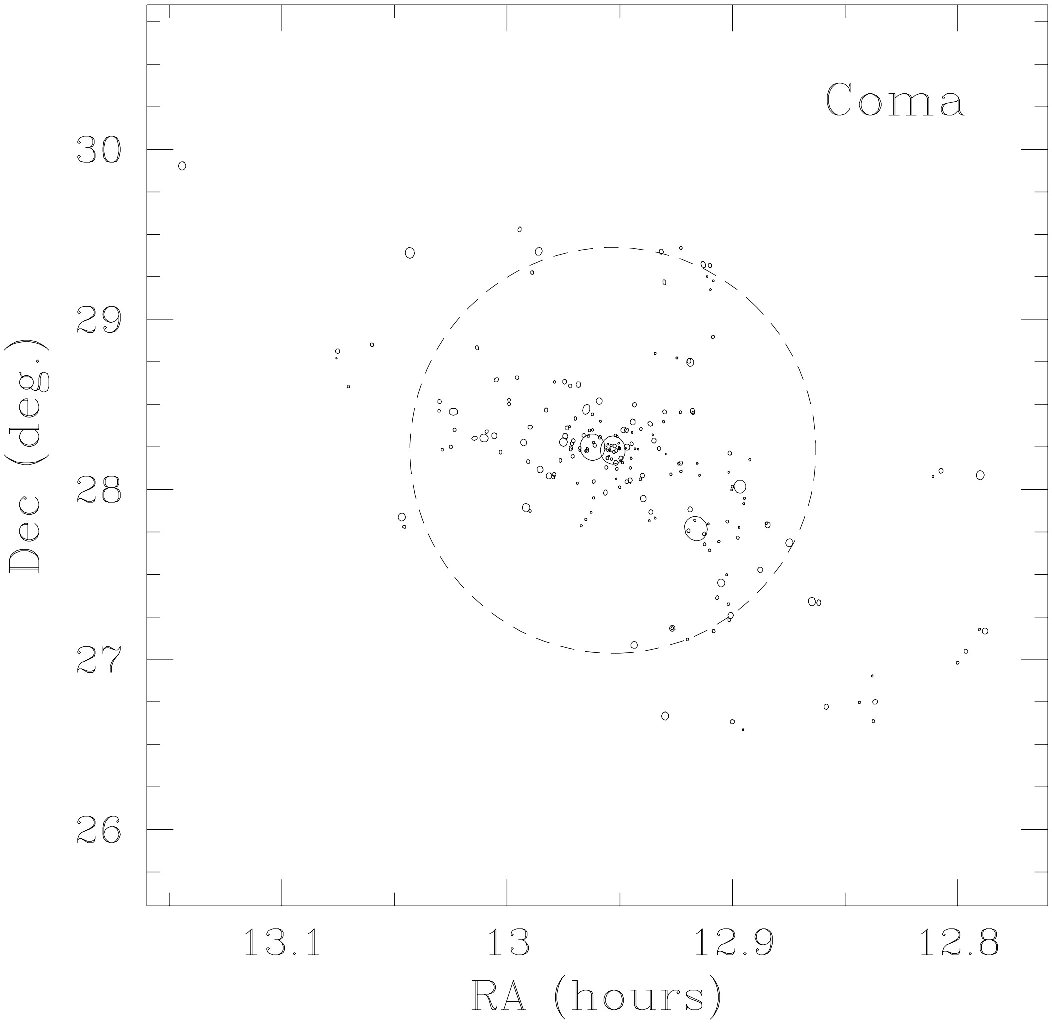

Figure 3.3 (Continued)

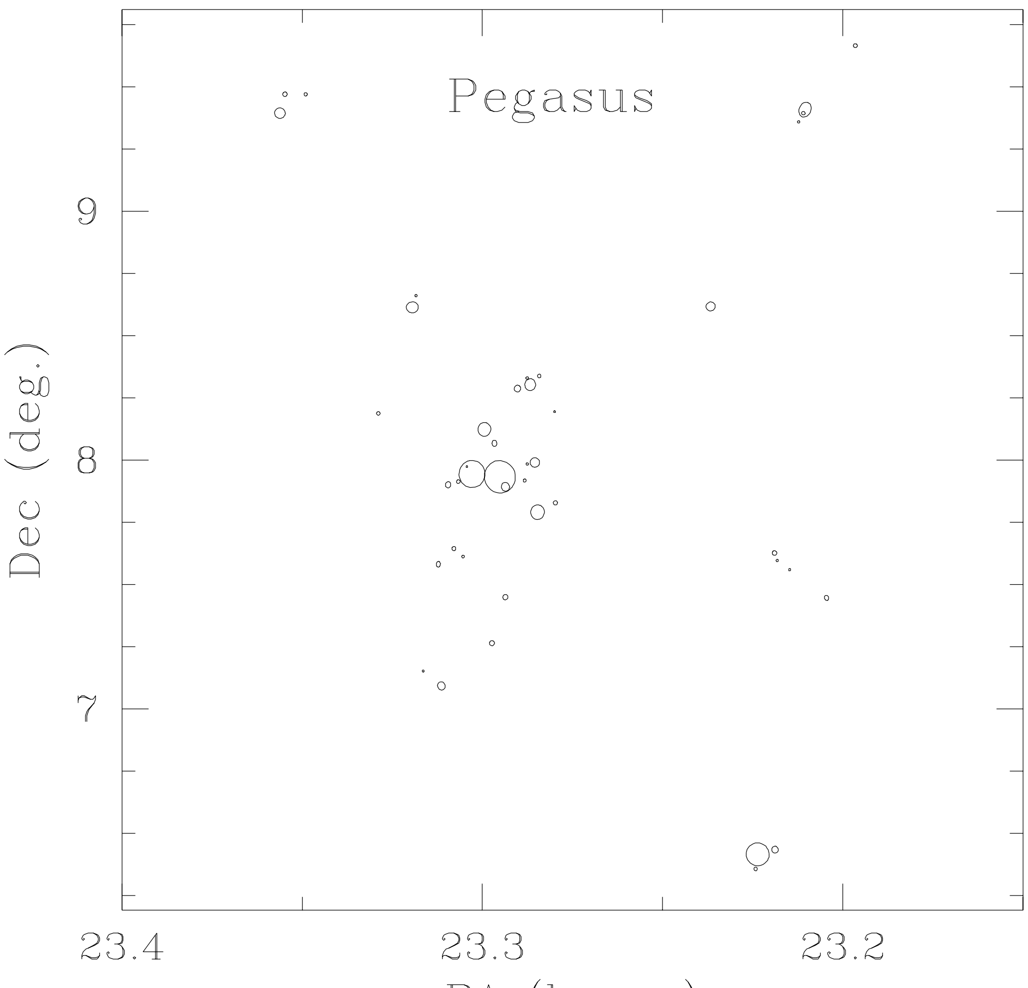

Figure 3.3 (Continued)

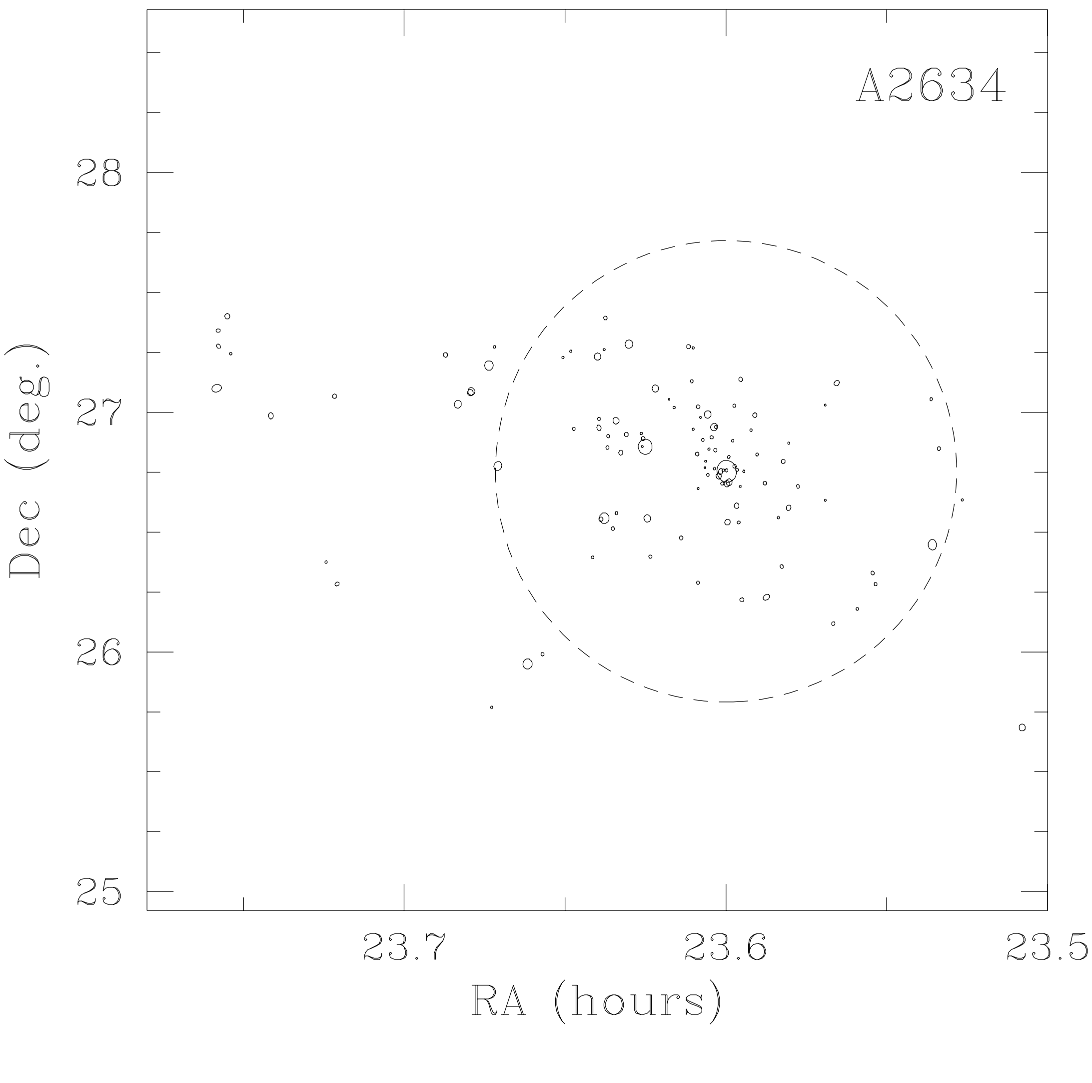

(Zwicky *et al.* 1963-1968). For galaxies in the Coma cluster that are not listed in either one of those catalogs, the Dressler number (Dressler 1980b) is given, if the galaxy is listed in that catalog.
Cols. 4 and 5: Right Ascension and Declination, in 1950.0 epoch.
Col. 6: morphological type code, in the RC3 (de Vaucouleurs *et al.* 1991) scheme (-5 for E, -2 for S0, 0 for S0a). Morphological types were derived from visual inspection of the blue plates of the Palomar Observatory Sky Survey (POSS). A few objects originally classified as S0 had their type revised to Sa after inspection of the CCD images.
Col. 7: Radial heliocentric velocity, in km s^{-1}.

3.2 Basic reduction

The data-reduction process has been performed entirely using standard and specially written IRAF procedures. All frames have been bias-subtracted, to remove the signal offset introduced by the read-out electronics, and then flat-fielded, to remove pixel-to-pixel sensitivity variations and any non-uniformity in the CCD illumination. At I band flat-fielding is a delicate operation. The CCD chip is somewhat transparent to I-band photons, and this makes its illumination pattern sensitive to the wavelength distribution (i.e. the color) of the incident light. Also, internal reflections and interference can take place during the exposure, producing small-scale structure in the illumination pattern of the CCD chip, known as "fringing". Dome flats, obtained pointing the telescope at a white, uniformly illuminated spot inside the dome, or twilight flats, obtained pointing at the evening or morning sky during twilight, do not quite reproduce the color of the night sky, or the fringing patterns, and cannot be used when high accuracy photometry is to be obtained. The best solution to this problem is to use the very same frames one is trying to flat-field. A large number of frames, taken over an interval of time of relative constancy of the camera and CCD setup, is combined using a median filtering technique (at each pixel the median value of the intensities measured in the frames being combined is recorded in the output image). Star and galaxy images are distributed almost randomly on these frames, and generally they occupy only a small fraction of the area of each frame. Therefore at each pixel the median value of the combination is very close to the sky background value, provided the number of frames being combined is large ($>$ 40 frames). Median filtering then allows an image of the uniform sky background to be obtained, here referred to as a "superflat". Dividing all frames by the superflat (properly normalized) eliminates fringing, non uniformity in the CCD illumination, and pixel-to-pixel sensitivity variation effects, providing satisfactory flat-fielding.

At this point, for ease of manipulation, one small frame (512 x 512 pixels) for each galaxy has been extracted from the 2048 x 2048 KPNO pixel frames. The 1024 x 1024 pixel MDM frames have been kept as single frames. The sky background has been subtracted from all frames, using the average number of counts measured in 10–12 "empty-sky"' regions. The typical number of pixels over which this average is computed is 30,000. The uncertainty in the subtracted background can be estimated from a comparison of the independent values subtracted from different frames extracted from the same 2048 x 2048 pixel frame. This uncertainty is typically of 0.2%. All pixels contaminated by the light of foreground stars or other galaxies, or by "cosmic rays hits" (energetic particles passing through the CCD chip leave behind ionization trails that simulate intense illumination on a small number of pixel) have been blanked and excluded from the final steps of surface photometry.

For galaxies severely contaminated by the light of a nearby object (either another galaxy or a foreground star), an iterative subtraction procedure has been used to obtain the individual light profiles. First, the brighter object has been fitted, after blanking the fainter one(s). The fit has been used to build a model of the object, which then has been subtracted from the original image. The subtracted image has been used to fit the fainter object, and again the fit has been used to build a model of it. The latter has then been subtracted from the original image, and the bright object has been fitted again. The procedure converges usually at the second iteration, producing companion-subtracted light profiles, although the uncertainty on the surface brightness distribution of these objects is higher than in other cases. This photometric approach is necessary, especially in the inner parts of clusters, where the galaxy density is high.

3.3 Photometric Calibration

The photometric calibration has been obtained with observations of Landolt standard stars (Landolt 1992). One or two Landolt fields were repeatedly observed during each night, at airmasses between 1.2 and 2.5, to provide an estimate of the photometric zero point and of the atmosphere extinction coefficient. Observations at I and R band were used to obtain a complete, color corrected, photometric solution. If $I_\circ$ and $R_\circ$ indicate the star true magnitude, and I and R indicate the magnitude measured at airmass X, then

$$I_\circ = I + \alpha_I X + \beta_c(R - I) + Z_I \tag{3.1}$$

$$R_\circ = R + \alpha_R X + \beta_c(R - I) + Z_R \tag{3.2}$$

Typical uncertainties in the zero–point determination are 0.02 magnitudes, both at I and R band. All galaxy magnitudes have been computed assuming a constant R–I color of 0.70 for elliptical, S0, and S0a galaxies (see, for example, Fukugita, Shiasaku & Ichikawa 1995). The uncertainty introduced by this assumption is negligible, because the color term coefficient β_c is always very small (< 0.05). Galaxy observations were all obtained at $X < 1.3$, thereby reducing the uncertainty in the airmass term in equations (3.1) and (3.2).

Most observations were obtained in photometric conditions. Those that were not have been calibrated using either short exposure frames obtained in photometric conditions (run 2 was calibrated entirely in this way, using frames obtained during run 3), or taking advantage of the partial overlap among frames in the mapping grid (non-photometric nights in runs 4, 5, 7, 8 were calibrated using this technique). In either case a sample of 10–15 stars that are present in both the "photometric" and the "non-photometric" image is selected, and instrumental (i.e. non calibrated) magnitudes for all these stars are obtained in both images. After rejecting the obvious variable stars, the mean magnitude difference between the stars in the two images is computed, and this is added to the photometric zero-point appropriate for the image obtained in photometric conditions to derive a zero-point for the other image. The typical uncertainty of this process is $\simeq$0.025-0.035 magnitudes.

3.4 On the De Vaucouleurs $r^{1/4}$ photometric profile

The so-called $r^{1/4}$ relation is an empirical relation that often (but not always) provides a good fit to the observed surface brightness radial distribution of elliptical galaxies (De Vaucouleurs 1948). The flux per unit area Σ as a function of the radial (angular) distance from the galaxy center is given by:

$$\Sigma(r) = \Sigma_e \; dex\left(-3.33\left[(r/r_e)^{1/4} - 1\right]\right) = \Sigma_e \; exp\left(-7.67\left[(r/r_e)^{1/4} - 1\right]\right) \tag{3.3}$$

The numerical coefficient in the exponential is chosen so that r_e, the effective radius, is that enclosing half the light of the galaxy. Written in terms of magnitudes per square arcsecond the surface brightness profile is then given by

$$\mu(r) = -2.5\log\Sigma(r) = 8.325\left[(r/r_e)^{1/4} - 1\right] + \mu(r_e) \tag{3.4}$$

where $\mu(r_e) = -2.5\log\Sigma_e$. At $r = 0$ we have $\mu_0 = \mu(r = 0) = \mu(r_e) - 8.325$, and therefore

$$\mu(r_e) = \mu_0 + 8.325 \tag{3.5}$$

When we fit the photometric profile $\mu = \mu\left(r^{1/4}\right)$ with a straight line $\mu = a + br^{1/4}$, then $\mu_0 = a$ and $\mu(r_e) = \mu_0 + 8.325 = a + 8.325$. Since $r^{1/4} = \frac{1}{b}(\mu - a)$ then

$$r_e = \left[\frac{8.325}{b}\right]^4 \tag{3.6}$$

Integrating equation 3.3 from zero to infinity, we obtain for the galaxy total flux

$$\Sigma_{tot} = 7.214\pi r_e^2\Sigma_e \tag{3.7}$$

while the integration from zero to r_e gives

$$\Sigma(< r_e) = 3.608\pi r_e^2\Sigma_e \tag{3.8}$$

In magnitudes, equation 3.7 then becomes

$$m_{tot} = \mu(r_e) - 3.39 - 5\log r_e \tag{3.9}$$

while from equation 3.8 we find that the relation between the effective surface brightness μ_e and $\mu(r_e) = -2.5\log\Sigma_e$ is given by

$$\mu_e = \mu(r_e) - 1.393 \tag{3.10}$$

3.5 Surface photometry

Surface photometry has been obtained using the GALPHOT software package, written for IRAF/STSDAS[1] mainly by W. Freudling, J. Salzer and M. Haynes. A galaxy's

[1] STSDAS (Space Telescope Science Data Analysis System) is distributed by the Space Telescope Science Institute, which is operated by AURA, under contract to the National Aeronautics and Space Administration.

light distribution has been fitted with elliptical isophotes, using a modified version of the STSDAS *Isophote* package. The center, ellipticity and position angle of the ellipse are the fit free parameters, while the ellipse semi–major axis is incremented by a fixed fraction of its value at each step of the fitting procedure. The procedure is stopped when the fitted mean number of counts per pixel drops below the rms dispersion around the mean value. The fitted parameters yield a model of the galaxy, which has been used to compute integrated magnitudes as a function of semi-major axis. At this point the measured fluxes in counts per pixel have been transformed into magnitudes per square arcsecond, and all magnitudes have been calibrated, color–corrected, and corrected for atmospheric extinction.

The radial surface brightness profiles have been fitted with a de Vaucouleurs $r^{1/4}$ profile (equation 3.4), to determine effective radius and effective surface brightness. For all galaxies the fit has been performed from an inner radius twice as large as the seeing disk radius. The outer radius has been chosen depending on the shape of the surface brightness profile. For those objects that are well described by the $r^{1/4}$ law at all radii, the fit has been extended out to the outermost isophotes. For all other galaxies, only the central core has been fitted. No attempt has been made to fit simultaneously two components (like an $r^{1/4}$ bulge and an exponential disk) to these surface brightness profiles, since the FP relation is valid only for spheroidal systems. The effective radius r_e and the surface brightness at r_e are the two free parameters in the fit (see section 3.4 for details), and the effective surface brightness μ_e (the mean surface brightness within r_e) has been obtained from $\mu(r_e)$ as $\mu_e = \mu(r_e) - 1.392$ (this is strictly valid only for a galaxy that follows the $r^{1/4}$ profile at all radii). The median values for r_e and μ_e, measured over the entire sample, are 8.94 arcsec, and 20.97 magnitudes per square arcsec respectively. The formal uncertainty with which effective radius and effective surface brightness have been derived is given by the uncertainty of the $r^{1/4}$ fit. The median value for the uncertainty in r_e is 6.2%, and in μ_e is 0.08 magnitudes per square arcsec.

To compute total magnitudes the outer portion of the surface brightness profile of those galaxies not well represented by the $r^{1/4}$ law at all radii has been fitted using either a different $r^{1/4}$ profile from the one used to fit the core of the galaxy, or an exponential disk profile, depending on the profile shape. Then, in all cases (single $r^{1/4}$ fit, or double fit), the fit describing the outer parts of the galaxy has been extrapolated to infinity, and the flux corresponding to the extrapolated portion of the profile only has been computed. This flux has been added to the observed integrated flux within the radius of the outermost ellipse used in the fit, to give the galaxy total magnitude. The median uncertainty with which total magnitudes are derived is 0.06 magnitudes.

Total magnitudes and effective surface brightnesses have been corrected for Galactic extinction and cosmological effects. Extinction corrections have been taken from Burstein & Heiles (1978), using $A_I = 0.45 A_V$, and range from 0.0 to 0.13 mag. Cosmological K-corrections have been computed assuming $F_\nu \sim \nu^0$ (the energy distribution of early-type galaxies in the red is nearly flat) so that $K_I = 2.5 \log(1+z)$, and range from 0.01 to 0.04 mag. The $(1+z)^4$ cosmological corrections to surface brightness range from 0.04 to 0.15 mag. Effective radius and effective surface brightness have been corrected for the smearing effects of seeing, following the prescriptions of Saglia *et al.* (1993a, see in particular their Figure 8). The median seeing correction to r_e produces a reduction of 2% of its value. The median seeing correction to μ_e amounts to 0.016 magnitudes per square arcsec.

The parameters obtained from the surface photometry are listed in Table A.2 in the appendix. The table is organized as follows:
Col. 1: Galaxy name, as in Table A.1
Col. 2: Measured effective radius, in arcseconds.
Col. 3: Effective radius, in arcseconds, corrected for seeing effects.
Col. 4: Uncertainty on the effective radius, in arcseconds.
Col. 5: Corrected metric effective radius, in kiloparsec, obtained assuming the galaxy is at the distance indicated by the cluster redshift, in the CMB reference frame, for $H_\circ = 100$ km s^{-1}Mpc^{-1}.
Col. 6: Measured effective surface brightness, in I band magnitudes per square arcsecond.
Col. 7: Corrected effective surface brightness, in I band magnitudes per square arcsecond. μ_e is corrected for the smearing effects of seeing, for extinction within our Galaxy, for the cosmological k-correction term , and for the $(1+z)^4$ cosmological dimming.
Col. 8: Uncertainty on the effective surface brightness, in magnitudes per square arcsecond.
Col. 9: Apparent I band magnitude, corrected for extinction within our Galaxy, and for the cosmological k-correction term.
Col. 10: Absolute magnitude. This is obtained assuming that the galaxy is at the distance indicated by the cluster redshift, in the CMB reference frame, for $H_\circ$=100 km s^{-1}Mpc^{-1}.
Col. 11: Quality codes. The 3 one-digit codes provide information on the photometric quality of the observation, on the quality of the image, and on the shape of the photometric profile, respectively.
Photometric code: 1 = observation obtained in photometric conditions, uncertainty in the zero-point determination <0.03 mag; 2 = observation obtained in photometric conditions, uncertainty in the zero-point determination 0.03–0.05 mag; 6 = observation obtained in non-photometric conditions, uncertainty in the zero-point determination <0.03 mag; 7 = observation obtained in non-photometric conditions, uncertainty in the zero-point determination 0.03–0.06 mag.
Image quality code: 0 = image is OK; 1 = small amount of contamination from nearby stars or other galaxies; 2 = significant amount of contamination from nearby stars or other galaxies; 3 = iterative subtraction of the contaminating object required; 4 = flat-fielding of sub-standard quality, due to scattered light from a nearby bright star.
Profile code: 1 = $r^{1/4}$ fit good at all radii; 2 = $r^{1/4}$ fit acceptable at all radii; 3 = $r^{1/4}$ fit good only in the core of the galaxy; 4 = the $r^{1/4}$ fit does not provide an acceptable description of the observed photometric profile.
If an asterisk appears in this column, special comments on the object are included at the foot of the table.

3.6 Internal and external comparisons

Repeated observations of a small fraction of the galaxies listed in Table A.2 provide the opportunity to evaluate the internal consistency of the photometric measurements. In most cases the galaxies were observed twice, sometimes during the same night, some-

Table 3.2 Photometry internal comparison

Parameter	N	mean difference	rms scatter	mean uncertainty
$\log r_e$	71	-0.003	0.044	0.038
μ_e	71	-0.001	0.131	0.113
m_{tot}	71	0.071	0.087	0.084
$\log r_e - 0.32\mu_e$	71	0.000	0.020	0.010

times during separate nights of the same observing run, sometimes during different runs. In total, 71 pairs of observations are available. The results of the comparison of effective radius, effective surface brightness, and total magnitude are presented in Figure 3.4, and they are listed in Table 3.2. Also listed in this table are the mean statistical uncertainties associated with the derivation of those parameters, multiplied by a $\sqrt{2}$ factor to allow a direct comparison with the rms scatter in the observations (assuming equal error contributions to the rms scatter). There is good general agreement between the rms scatter derived from the comparison and the estimated statistical uncertainties, with the rms scatter being only marginally larger. This small difference could be due to residual uncertainties in the seeing corrections.

The errors on r_e and μ_e are highly correlated. Figure 3.5a shows $\Delta \log r_e$ versus $\Delta\mu_e$ for the 71 pairs of observations. The linear correlation coefficient for these differences is 0.962. This correlation has an important effect in reducing the uncertainty on the combination of $\log r_e$ and μ_e that is empirically found to enter the FP relation: $\log r_e - 0.32\ \mu_e$ (see Figure 3.5b). From the statistical uncertainties on $\log r_e$ and μ_e, and the observed correlation between them, it is possible to derive the expected uncertainty on $\log r_e - 0.32\ \mu_e$, which is 0.010. However, we must note that a small change in the linear correlation coefficient has a big effect on the computation of this expected uncertainty: a 10% difference in its value corresponds to a doubling of the $\log r_e - 0.32\ \mu_e$ expected uncertainty. The rms scatter from the comparison is 0.020. This can be considered to be in fair agreement with the predicted value, given the previous consideration.

The absolute accuracy of the photometric measurements can be verified using comparisons with similar measurements presented by Lucey *et al.* (1991b), Saglia, Bender & Dressler (1993b), Jørgensen, Franx & Kjærgaard (1995) for galaxies in the Coma cluster. Unfortunately none of these studies used I band for the photometric observations, and therefore it is necessary to assume standard colors for E and S0 galaxies, before comparisons can be made. The V band magnitudes from Lucey *et al.* (1991b), the B band magnitudes from Saglia, Bender & Dressler (1993b), and the Gunn r band magnitudes from Jørgensen, Franx & Kjærgaard (1995) have been transformed to I band magnitudes using V–I, B–I, and r–I colors of 1.31, 2.25, and 1.07, respectively (Fukugita, Shiasaku & Ichikawa 1995). The expected rms scatter in the true colors of E and S0 galaxies around these mean values is $\simeq 0.1$ magnitudes.

There are 57 galaxies in common with the sample of Lucey *et al.* (1991b), 47 with

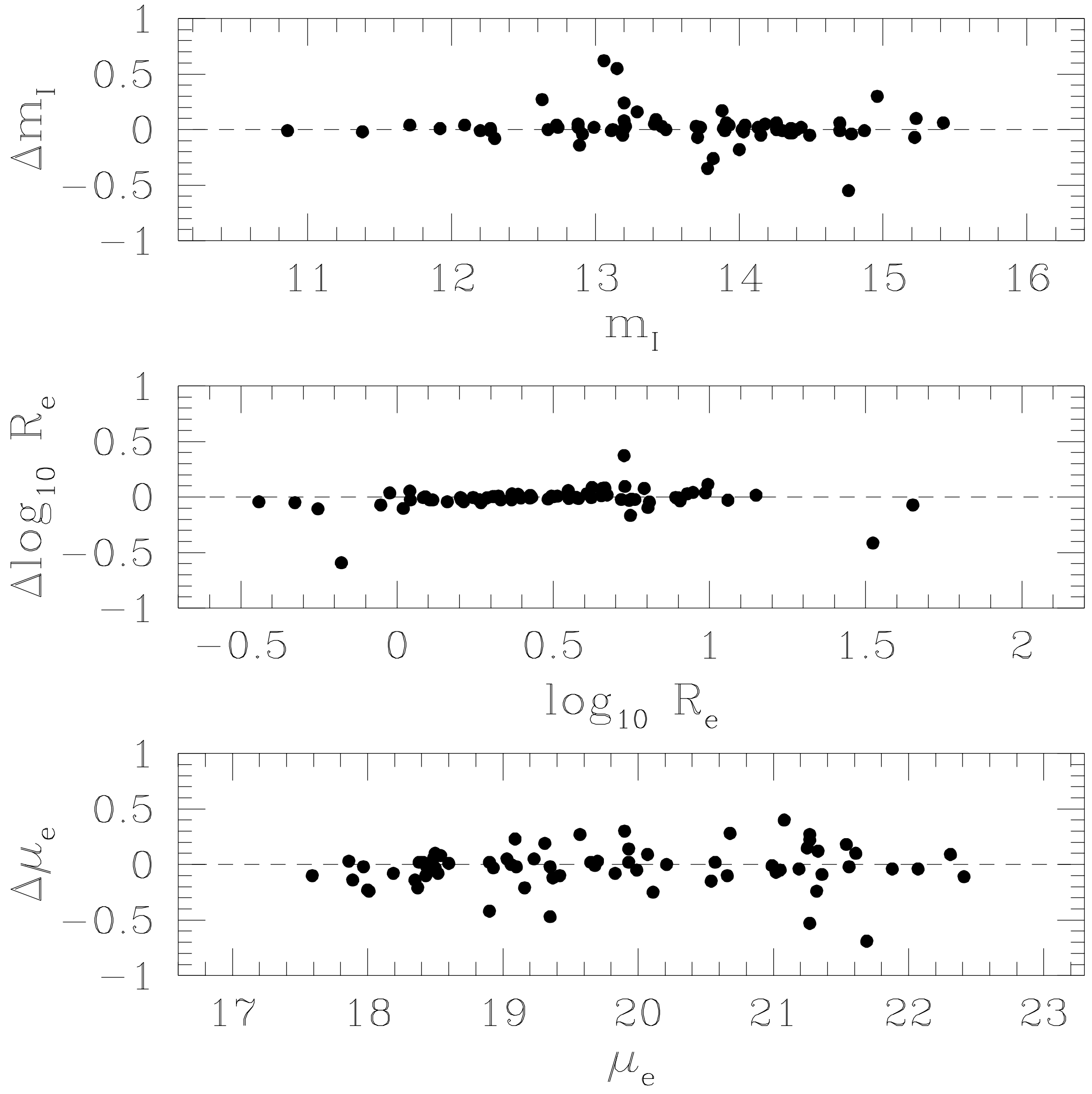

Figure 3.4 Internal comparison of the global photometric parameters. Δm_I, $\Delta log_{10} R_e$, and $\Delta \mu_e$ are the differences between the values of the total magnitude, effective radius, and effective surface brightness obtained from repeated observations of 71 galaxies.

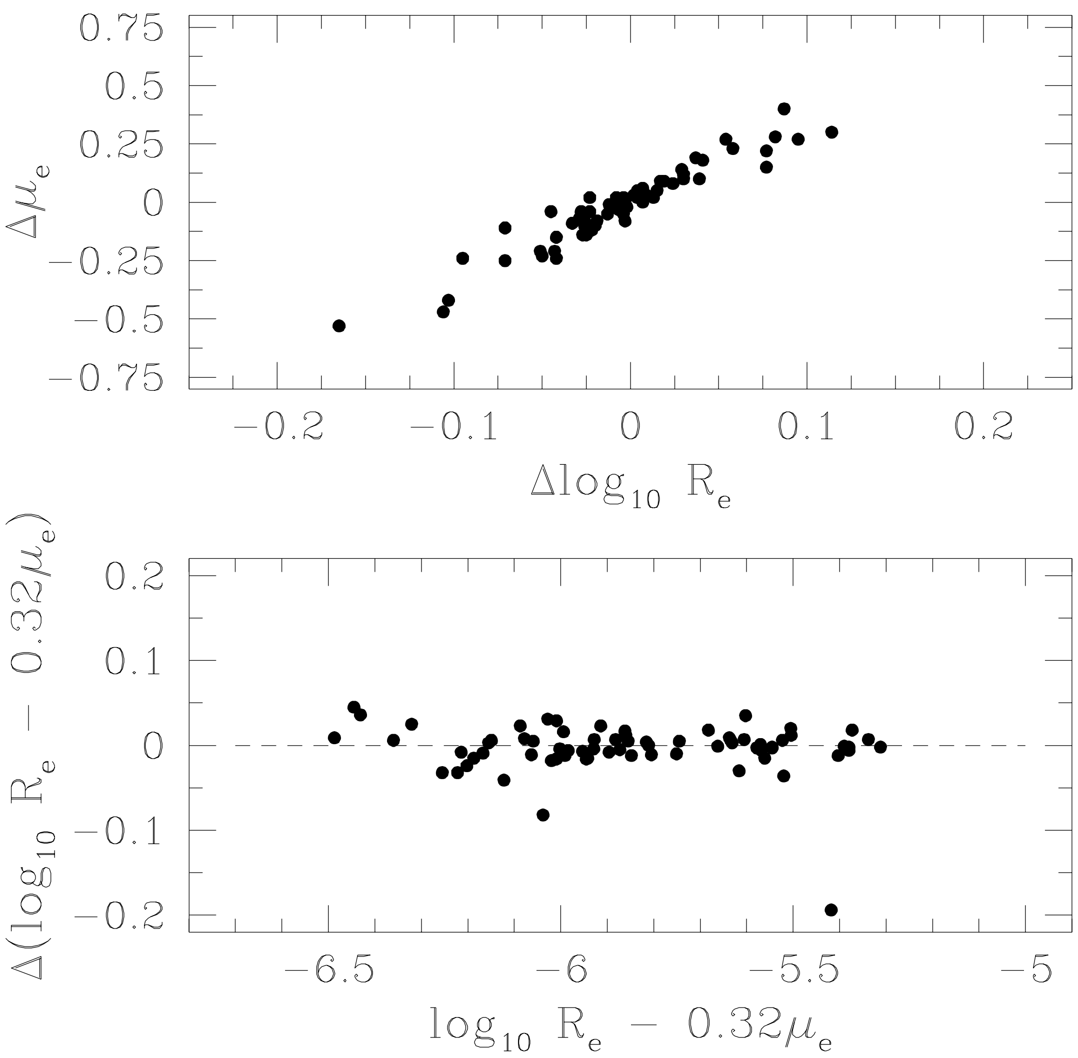

Figure 3.5 (a) The correlation of the errors in $\log r_e$ and μ_e. The figure shows the differences measured from repeated observations. The linear correlation coefficient for this data-set is 0.962. (b) Internal comparison of the combination $\log r_e - 0.32\,\mu_e$, which is the combination that enters in the FP relation.

Table 3.3 Photometry external comparison

Parameter	N	mean difference	rms scatter
	Saglia et al. (B band)		
$\log r_e$	47	0.158	0.240
μ_e	47	0.365	0.813
$\log r_e - 0.32\mu_e$	47	0.034	0.043
	Lucey et al. (V band)		
$\log r_e$	57	0.030	0.100
μ_e	57	-0.100	0.353
$\log r_e - 0.32\mu_e$	57	0.060	0.030
	Jørgensen et al. (r band)		
$\log r_e$	106	0.173	0.248
μ_e	106	0.438	0.741
$\log r_e - 0.32\mu_e$	106	0.031	0.038

the sample of Saglia, Bender & Dressler (1993b), and 106 with the sample of Jørgensen, Franx & Kjærgaard (1995). Table 3.3 and the panels of Figure 3.6 show the results of the comparisons of effective radius, effective surface brightness, and the combination $\log r_e - 0.32\ \mu_e$. There are significant differences in the determinations of both the effective radius and the effective surface brightness. However it is possible to show that the main source of these differences is in the different procedures adopted to perform the $r^{1/4}$ fit, and in particular in the choice of what portion of the photometric profile to use for the fit. In this work the fit was performed to an outer radius which was chosen on the basis of the shape of the photometric profile: for profiles that do not follow the $r^{1/4}$ relation at all radii, only the core of the galaxy was fitted. If the fit were to be performed using all the points in the photometric profile, the fitted profile would have a different slope, and both the effective radius and the effective surface brightness would have different values. This is the main source of discrepancy with the works of Saglia, Bender & Dressler (1993b), and of Jørgensen, Franx & Kjærgaard (1995). Panels (a) and (c) of Figure 3.6 show with filled symbols the galaxies whose photometric profile follows the $r^{1/4}$ relation at all radii, and with empty symbols those galaxies that do not. It is clear that the largest discrepancies are mostly associated with the latter objects. Another possible source of discrepancy is the choice of the inner radius from where to start the $r^{1/4}$ fit. In this work this radius is chosen to be twice the radius of the seeing disk. A different choice would lead again to a fitted profile with somewhat different slope, especially for objects with small effective radius. Because these differences in $\log r_e$ and μ_e originate from differences in the $r^{1/4}$ fit, they are correlated precisely as the errors in $\log r_e$ and μ_e are. This is shown by the excellent agreement in the comparison of the combinations $\log r_e - 0.32\ \mu_e$. It is therefore possible to say that these external comparisons show good overall agreement, and confirm the quality of the photometric measurements presented in this work.

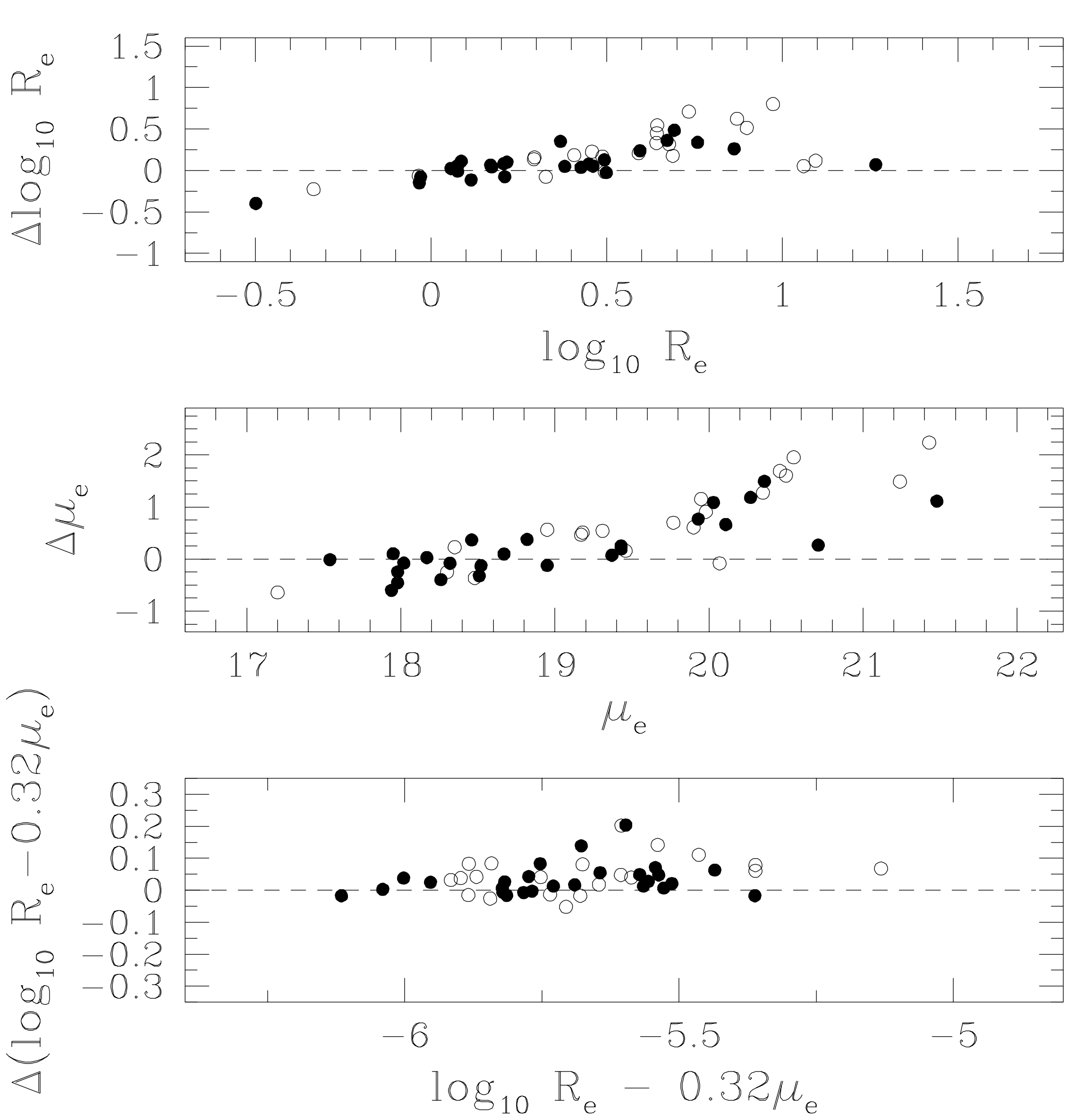

Figure 3.6 External comparison of the global photometric parameters for galaxies in the Coma cluster. (a) Comparison with the B band data from Saglia et al. (1993b). (b) Comparison with the V band data from Lucey et al. (1991b). (c) Comparison (c) with the r band data of Jorgensen et al. (1995). B, V, and r magnitudes were converted to I magnitudes for the comparison, using fixed B-I, V-I and r-I colors (see text).). Panels (a) and (c) show with filled symbols the galaxies whose photometric profile follows the $r^{1/4}$ relation at all radii, and with empty symbols those galaxies that do not.

Figure 3.6 (Continued)

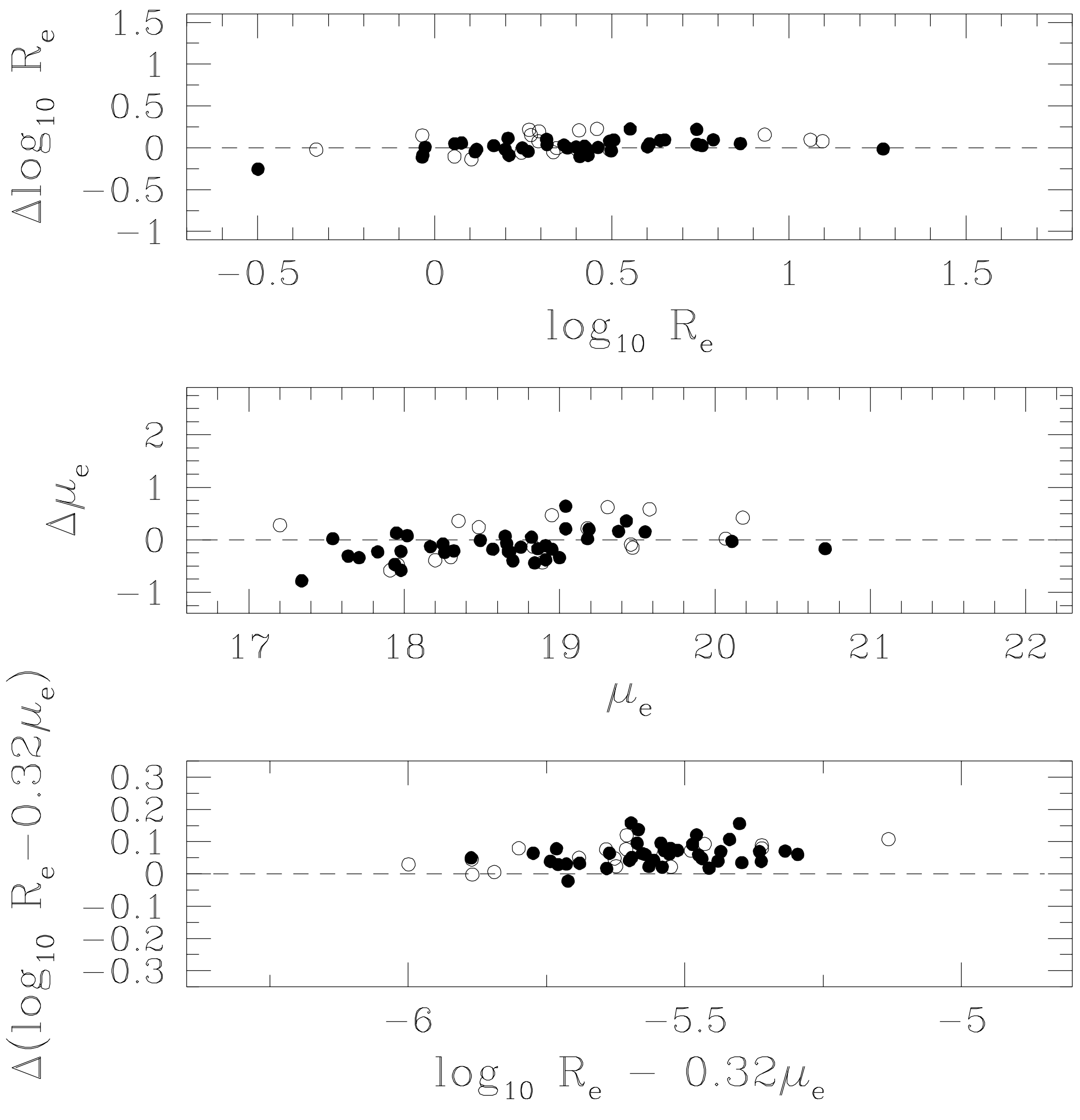

Figure 3.6 (Continued)